Journal of Polymer Research (2023) 30:141
https://doi.org/10.1007/s10965-023-03519-7

ORIGINAL PAPER

Urethane-acrylate-based photo-inks for digital light processing of flexible materials

Guanxing Kuang[1] · **Hadi Bakhshi**[1,2] · **Wolfdietrich Meyer**[1,2]

Received: 8 December 2022 / Accepted: 7 March 2023 / Published online: 21 March 2023

Abstract

Urethane–acrylate-based photo-inks containing various concentrations (0.1–1.5 wt.%) of two photo-initiators, namely ethyl phenyl(2,4,6-trimethylbenzoyl)phosphinate (TPOL) or diphenyl(2,4,6-trimethylbenzoyl)phosphine oxide (BPO), for digital light processing (DLP) were developed. According to photo-DSC kinetics investigations, no significant difference was detected between the photo-activity of formulations containing BPO or TPOL at various concentrations. BPO (1.0 wt.%) with a high molar extinction coefficient (500 L/mol·cm at 365 nm) resulted in higher controllability on the layer thickness (100 µm) during the 3D printing process. The surface cracks that appeared during the post-curing process could be avoided by splitting the exposure time (5 min) into short intervals (5 × 1 min) without affecting double bond conversion (*DBC*). Several flexible objects were successfully 3D printed in good quality and their thermomechanical properties and layer-by-layer morphology were investigated.

Keywords 3D printing · Photo-initiator · Photo-curing · 3D Printability, Tensile properties

Introduction

3D printing technology, called also additive manufacturing (AM), is a process of joining materials layer-by-layer to produce complex objects without molding or machining [1]. The photo-polymerization-based 3D printing technologies such as stereolithography (SLA), digital light processing (DLP), liquid crystal precision (LCP), and digital light synthesis (DLS) or continuous liquid interface production (CLIP) enable the fabrication of customized/complex multifunctional 3D objects with controlled chemical and mechanical properties [2, 3]. In the DLP technology, a light pattern is projected to a photo-curable ink (photo-ink) to solidify it in the *X*-/*Y*-directions with a defined depth and attach it to a building stage. In the next step, The building stage is lifted up/down in the *Z*-direction by a defined height allowing the liquid photo-ink to wet the surface of the solidified layer. The photo-curing depth (C_d) of the photo-ink is slightly larger than the defined thickness layer (Δz) to ensure proper chemical/physical adherence between the layers [4–6]. Therefore, C_d determines the Δz limits and consequently the *Z*-resolution for the DLP process, which is in the range of 10–200 µm [5].

The 3D printing photo-inks are formulations of monomers/oligomers and photo-initiators, which are converted from liquid to solid under exposure to light with a specific wavelength. The irradiation wavelength and intensity of the 3D printer light source play an important role in formulating the photo-inks, especially in choosing photo-initiators. The type and concentration of photo-initiators are adjusted with the 3D printing parameters to ensure a high 3D printing quality.

Mono(acyl)phosphine and bis(acyl)phosphine oxides are commonly used as photo-initiators in photo-inks due to their superior characteristics. Upon light irradiation, an α-cleavage reaction occurs for mono(acyl)phosphine oxides under triplet-state to produce benzoyl and phosphinoyl radicals (Scheme 1a). For bis(acyl)phosphine oxides, the α-cleavage generates benzoyl and phosphinoyl oxide radicals (Scheme 1b). The addition of the phosphinoyl oxide radical to the monomers leads to a macro-mono(acyl)

✉ Hadi Bakhshi
hadi.bakhshi@iap.fraunhofer.de

[1] Department of Functional Polymer Systems, Fraunhofer Institute for Applied Polymer Research IAP, Geiselbergstraße 69, 14476 Potsdam, Germany

[2] Department of Life Science and Bioprocesses, Fraunhofer Institute for Applied Polymer Research IAP, Geiselbergstraße 69, 14476 Potsdam, Germany

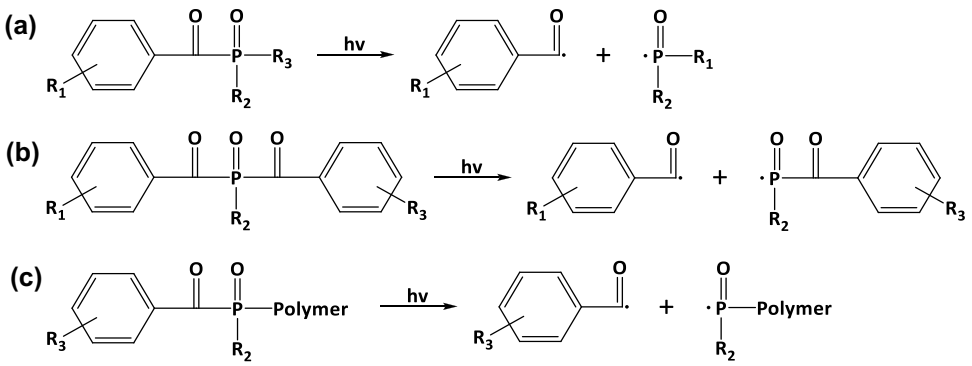

Scheme 1 The α-cleavage for mono(acyl)phosphine oxides (**a**) and bis(acyl)phosphine oxides (**b**) and the second α-cleavage of macro-mono(acyl)phosphine (**c**) upon light irradiation [7]

phosphine oxide, which can undergo a second α-cleavage reaction to form another benzoyl and macro-phosphinoyl radicals (Scheme 1c) [7, 8].

In this research, the photo-curing kinetics and Jacob's working curve theory are combined to optimize the photo-initiators in the urethane–acrylate-based photo-inks for DLP 3D printing. Ultraviolet–Visible (UV–Vis) spectroscopy was done to obtain the absorption spectra of photo-initiators, namely ethyl phenyl(2,4,6-trimethylbenzoyl)phosphinate (TPOL) and diphenyl(2,4,6-trimethylbenzoyl)phosphine oxide (BPO or Irgacure 819). Differential scanning photo-calorimetry (photo-DSC) and DLP 3D printing were carried out to evaluate the influence of photo-initiator concentration on photo-polymerization. Furthermore, the DLP 3D printing parameters such as irradiation intensity, exposure time, and post-curing process were optimized to ensure the printability of the optimized photo-ink. Based on the optimized parameters, several CAD models were printed to verify the quality and accuracy of the DLP 3D printing process. In the end, the thermomechanical properties and layer-by-layer structure of the 3D printed objects were evaluated.

Experimental

Materials

7,7,9(or 7,9,9)-trimethyl-4,13-dioxo-3,14-dioxa-5,12-diazahexadecane-1,16-diyl bismethacrylate (UrDMA) and 2-[[(butylamino)carbonyl]oxy]ethyl acrylate (UrA) were used as monomers. Ethyl phenyl(2,4,6-trimethylbenzoyl) phosphinate (TPOL) and diphenyl(2,4,6-trimethylbenzoyl) phosphine oxide (BPO) were used as photo-initiators. Analytical grade isopropanol and acetonitrile were obtained from Sigma-Aldrich (Germany).

3D printing process

Formulations based on UrDMA/UrA (40/60, 30/70, or 20/80, wt./wt.) containing TPOL or BPO (0.5, 1.0, or 1.5 wt.% of total monomers' mass) were prepared as photo-inks. The 3D printability of the photo-inks was evaluated on a DLP 3D printer (MiiCraft, MiiCraft Ultra 125x, Taiwan) operating at 365 nm. The *X*-/*Y*-resolutions were 65 µm and the *Z*-axis layer thickness was set as $\Delta z = 100$ µm. After 3D printing, samples were removed from the build plate, washed twice with fresh isopropanol in an ultrasonic bath (BANDELIN electronic GmbH & Co. KG, Sonorex Super RK 102H, Germany) for 5 min, and dried by a compressed air blowgun. The washed samples were post-cured under a high-intensity UV lamp (Dr. Hönle AG, UVAHAND 250, Germany) for different times.

Instruments

UV–Vis spectroscopy of monomers and photo-initiator solutions in acetonitrile (0.8 g/L) was done using a PerkinElmer instrument (Lambda 950, USA) operating in the range of 200–700 cm^{-1}. Acetonitrile was used as a blank solution.

A Netzsch machine (DSC 204 F1 Phoenix, Germany) equipped with a spot UV curing system (Lumen Dynamics, OmniCure® S2000, Canada) was employed to evaluate the photo-curing of the formulations through differential scanning photo-calorimetry (photo-DSC). The experiments were done in an isothermal mode at 25 °C with a uniform UV intensity of 0.1 mW/cm^2 under an N_2 atmosphere (40 mL/min). The irradiation step was prolonged for 3 min to fully photo-cure the samples and reach a plateau region, which was employed as a baseline for the peak integrations. The reported values are an average of at least three measurements.

The thermal transitions of monomers were evaluated by differential scanning calorimetry (DSC, Netzsch, DSC 204 F1 Phoenix, Germany) in the range of -100 to 100 °C at a heating rate of 10 °C/min under an N_2 atmosphere (40 mL/min). The glass transition temperatures (T_g) were extracted from the middle point of the baseline change in the first heating cycle. The crystallization (T_c) and melting (T_m) temperatures were extracted from the onset of the corresponding peaks.

A Thermo Fisher Scientific spectrometer (Nicolet™ iS20) equipped with an attenuated total reflection (ATR) unit (PIKE Technologies, GladiATR™) was used to record the Fourier-transform infrared (FTIR) spectra of the photo-inks and 3D printed samples in the range of 4000–400 cm^{-1} at a 4 cm^{-1} resolution with 32 scans.

The layer-by-layer structure of the 3D printed samples was studied by scanning electron microscopy (SEM, Zeiss, GeminiSEM 300, Germany) at a standard accelerating voltage of 5 kV. An Everhart–Thornley detector (SE2) and an InLens detector (IL) were used as secondary electron detectors. Samples were coated with gold before microscopy.

A Zwick/Roell machine (Z020, Germany) was employed for investigating the tensile properties of the 3D printed bone-shaped specimens (ASTM D638 Type IV) according to ISO 527–1:2019. The load cell was 10 KN, the clamping length was 34 mm, the pre-load was 0.05 N, and the crosshead speed was 19 mm/min. The reported values are an average of at least three specimens for each sample.

Thermogravimetric analysis (TGA) was done on a Mettler Toledo instrument (TGA 2). The heating rate was 10 °C/min from 20 to 600 °C under N_2 flow at a rate of 50 mL/min.

Methods

The photo-curing rate (R_p, *1/s*) and double bond conversion (*DBC*, %) as a function of time were calculated from photo-DSC data using Eqs. (1)–(3) [9, 10];

$$\Delta H_{theor} = \frac{f \cdot n \cdot \Delta H_0}{M_w} \tag{1}$$

$$R_p = \frac{dH_p}{dt} / \Delta H_{theor} \tag{2}$$

$$DBC = \frac{\Delta H_p}{\Delta H_{theor}} \times 100 \tag{3}$$

where ΔH_{theor} (J/g) is the theoretical total heat released during the complete polymerization of the monomers within the sample, f is the mass fractions of each monomer within the sample, n is the number of double bonds in each monomer, ΔH_0 (J/mol) is the standard heat of polymerization for methacrylate (54.8 kJ/mol [9]) or acrylate (86.2 kJ/mol [9]), M_w (g/mol) is the molecular weight of each monomer, dH_p/dt (J/s·g or W/g) is the normalized heat flow per second, and ΔH_p (J/g) is the heat released from the start of photo-curing up to a certain time obtained from the integration of DSC thermograms.

The photo-curing depth of formulations was determined on a DLP 3D printer. For this purpose, each formulation was dropped on a glass slide (Fig. S1 in Supplementary Information, SI) and exposed to different UV (365 nm) intensities and exposure times. Then, the remaining liquid photo-ink was wiped off so that only a solid photo-cured layer was left on the glass slide. The thickness of the layer was determined by a digital external micrometer.

Statistical analysis

The results expressed as mean ± SD are representing at least three independent experiments. The differences between groups were analyzed using the one-way ANOVA and LSD test for multiple comparisons ($p < 0.05$: significant difference).

Results and discussion

UV–Vis absorption

Optimizing the photo-initiator within photo-inks is essential for the 3D printing application. Many parameters influence the performance of a photo-initiator such as dissociation quantum yield, light absorption in terms of molar extinction coefficient and absorption wavelength, rate constant for the addition of the generated radicals to monomers, and side reactions like oxygen quenching [11]. The chemical structures of TPOL and BPO are depicted in Scheme 1. TPOL is a liquid mono(acyl)phosphine oxide with high solubility that can be mixed easily with most photo-inks, while BPO is solid bis(acyl)phosphine oxide with low solubility in photo-inks, especially at high concentrations, *e.g.* 4 wt.% [12]. The dissociation quantum yield (Φ) for TPOL and BPO are 0.3 [13] and 0.6 [8], respectively.

The photo-initiator molecules absorb the UV light, convert to their excited state, and generate free radicals. The UV–Vis spectra of TPOL and BPO were recorded in acetonitrile solution (0.8 g/L, Fig. 1a). TPOL showed absorption in the range of 200–420 nm with two maximums at 273 and 371 nm. BPO showed absorption in the range of 200–440 nm with two maximums at 295 and 369 nm. The second absorptions at 371 and 369 nm for TPOL and BPO, respectively, make them photo-active for the commercial DLP 3D printers mainly functioning at 365 nm. Meanwhile, both UrDMA and UrA monomers acetonitrile solution (0.8 g/L) were transparent in the region of 280–700 nm, which makes the whole irradiated light accessible for the photo-initiator molecules during the photo-curing process.

According to Lambert–Beer law, the absorbance (A) is given by Eq. (4) [14].

$$A = \varepsilon \cdot c \cdot l \tag{4}$$

where ε is the molar extinction coefficient, c is the molar concentration of the solution, and l is the path length. The molar extinction coefficient as a function of wavelength

was calculated for photo-initiators (Fig. 1b). BPO showed a larger molar extinction coefficient than TPOL, especially in the wavelength region of 320–440 cm^{-1}. A larger molar extinction coefficient for the photo-ink corresponds to a low light penetration depth and allows a more controllable 3D printing process and avoids over-cure as much as possible [15]. Thus, BPO is expected to provide higher photo-activity for the photo-inks compared with TPOL due to its enhanced dissociation quantum yield (0.6 [8]) and molar extinction coefficient (500 L/mol·cm at 365 nm). However, low solubility in the photo-inks is the main drawback of BPO as it is impossible to fully dissolve it at high concentrations, *e.g.* 4 wt.% [12].

Photo-curing

UrDMA as a viscous di-functional monomer (η = 9500 mPa·s) was used as a crosslinker in photo-inks to improve the dimensional stability of the 3D printed objects by generating a thermoset network structure [9, 16]. DSC analysis showed that UrDMA is a completely amorphous monomer with a glass transition temperature (T_g) of -33 °C and no melting point (Fig. S2 in SI). This is due to the existence of two enantiomers for UrDMA4, which prevents the packing and crystallization of UrDMA molecules (Scheme 2). Mono-functional UrA (η = 35 mPa·s) was employed as a reactive diluent to decrease the viscosity of photo-inks while resulting in flexibility for the 3D printed objects [9, 17]. According to DSC results, UrA is a semi-crystalline monomer with T_g of -81 °C and a melting point (T_m) of 5 °C (Fig. S3 in SI).

As mentioned, due to higher dissociation quantum yield and molar extinction coefficient values, BPO could provide higher photo-activity for the photo-inks compared with TPOL. Meanwhile, BPO as a bis(acyl)phosphine could be more effective due to the generation of four radicals compared with TPOL as a mono(acyl)phosphine oxide leading to two radicals.

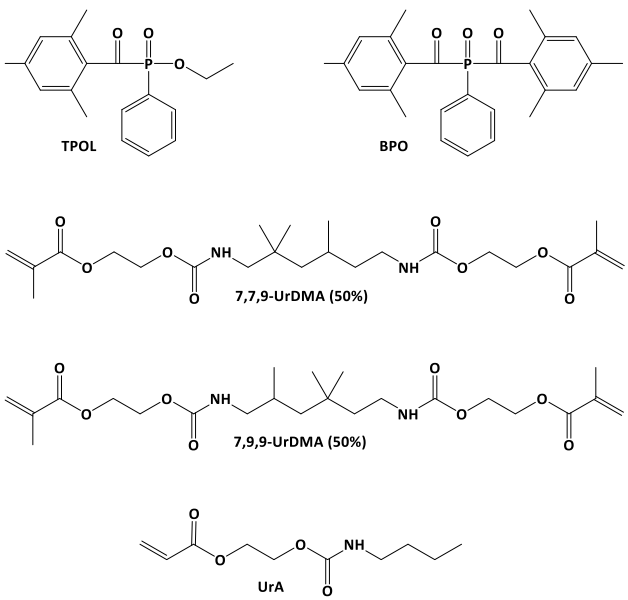

Scheme 2 The chemical structure of photo-initiators and monomers

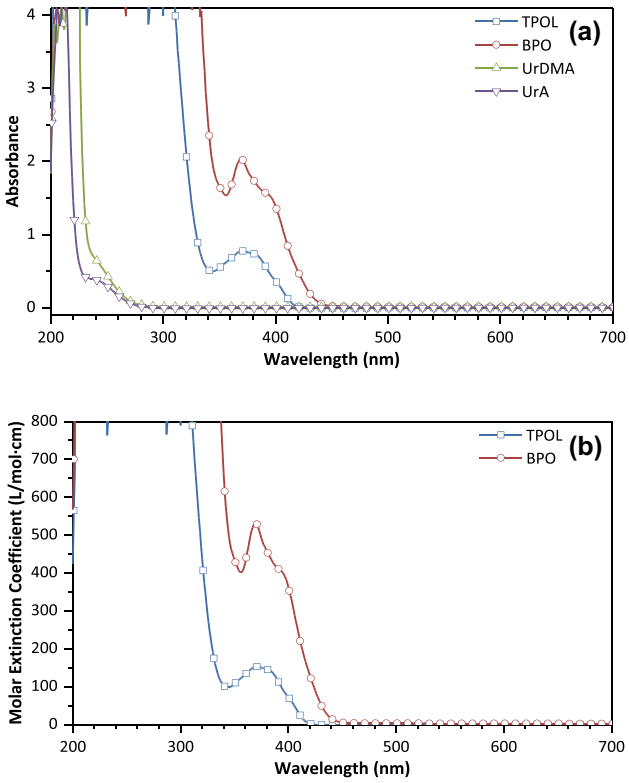

Fig. 1 UV–Vis absorption (**a**) and calculated molar extinction coefficient (**b**) as a function of wavelength for photo-initiators and monomers in acetonitrile solution (0.8 g/L)

Photo-DSC has been widely utilized to evaluate the photo-activity of 3D printing photo-inks [9]. The photo-polymerization kinetics of formulations based on UrDMA/UrA (40/60, wt./wt.) containing TPOL or BPO (0.5, 1.0, or 1.5 wt.% of total monomers' mass) was studied in the isothermal mode at 25 °C (Figs. S4 and S5 in SI). For all formulations, the curve of R_p versus photo-curing time showed an initial increase and a late decrease, known as the auto-acceleration and auto-deceleration phenomena, respectively, which is due to the gradual increase of viscosity with conversion and subsequent decrease of molecular mobility for monomers and macroradicals within the photo-curing mixture over time [9]. At low viscosity, R_p is constant and dependent on the double bonds' activity (chemistry-controlled). At middle viscosity (up to conversions of 11–13%), when the coupling of macroradicals for the termination is diffusion-limited but the monomers are still mobile, R_p increases (auto-acceleration). At high viscosity, when the photo-curing mixture is transforming into

a rubbery/glassy network (gel point) and the diffusion of monomers is significantly restricted, R_p decreases (auto-deceleration) [9].

The influence of the photo-initiator type and concentration on the photo-polymerization kinetic parameters such as the maximum photo-curing rate ($R_{p,max}$), the time to reach $R_{p,max}$ known as gel point time (t_{GP}), the conversion observed at $R_{p,max}$ known as gel point conversion (DBC_{GP}), and total double bound conversion (DBC_{total}) (Fig. 2 and Table S1 in SI). Both TPOL- and BPO-based formulations displayed fast photo-curing and high conversion. Increasing the photo-initiator concentration from 0.1 to 1.0 wt.% resulted in a partial improvement in R_p and further increasing to 1.5 wt.% led to a partial reduction in R_p (Fig. 2a), while the other kinetic parameters (t_{GP}, DBC_{GP}, and DBC_{total}) were not significantly changed ($p > 0.05$). On reason for lower R_p values at high photo-initiator concentration (1.5 wt.% compared to 1.0 wt.%) can be due to the major photon absorption at the top of the sample and limited photon penetration into the depth of the sample. TPOL-based formulations displayed partially higher R_p, earlier gel point (lower t_{GP}), and higher conversion (DBC_{GP} and DBC_{total}) compared with the corresponding BPO-based formulations. It is in opposition to the expectation obtained from the lower dissociation quantum yield (0.3 [13]) and molar extinction coefficient (145 L/mol·cm at 365 nm) for TPOL. One reason can be the lower molecular weight of TPOL (316.38 g/mol) compared to BPO (418.17 g/mol) resulting in higher molar percentages at the same weight percentages. For example, formulation TPOL 1.0% contains 0.87 mol.% of photo-initiator, while formulation BPO 1.0% has 0.66 mol.% of photo-initiator.

3D printing

For 3D printing of high-quality objects, good chemical/physical adherence between the interfaces of the cured layers is essential, which requires a C_d higher than Δz ($C_d > \Delta z$). Photo-curing a layer of photo-ink up to the gel point does not provide sufficient stiffness to allow the continuous layer-by-layer joining process [5]. As a result, DBC at the layer interface should be slightly higher than DBC_{GP}. Meanwhile, very high C_d can cause overexposure ($C_d \gg \Delta z$) and unintended photo-curing of space-filling features, *e.g.* porous inclusions [5]. Furthermore, if $C_d = \Delta z$, the layer-by-layer joining process can fail due to poor adherence between the sequentially photo-cured layers [5].

C_d can be regulated by changing the photo-initiator concentration, irradiation intensity, and exposure time. At low photo-initiator concentration, a minor fraction of photons

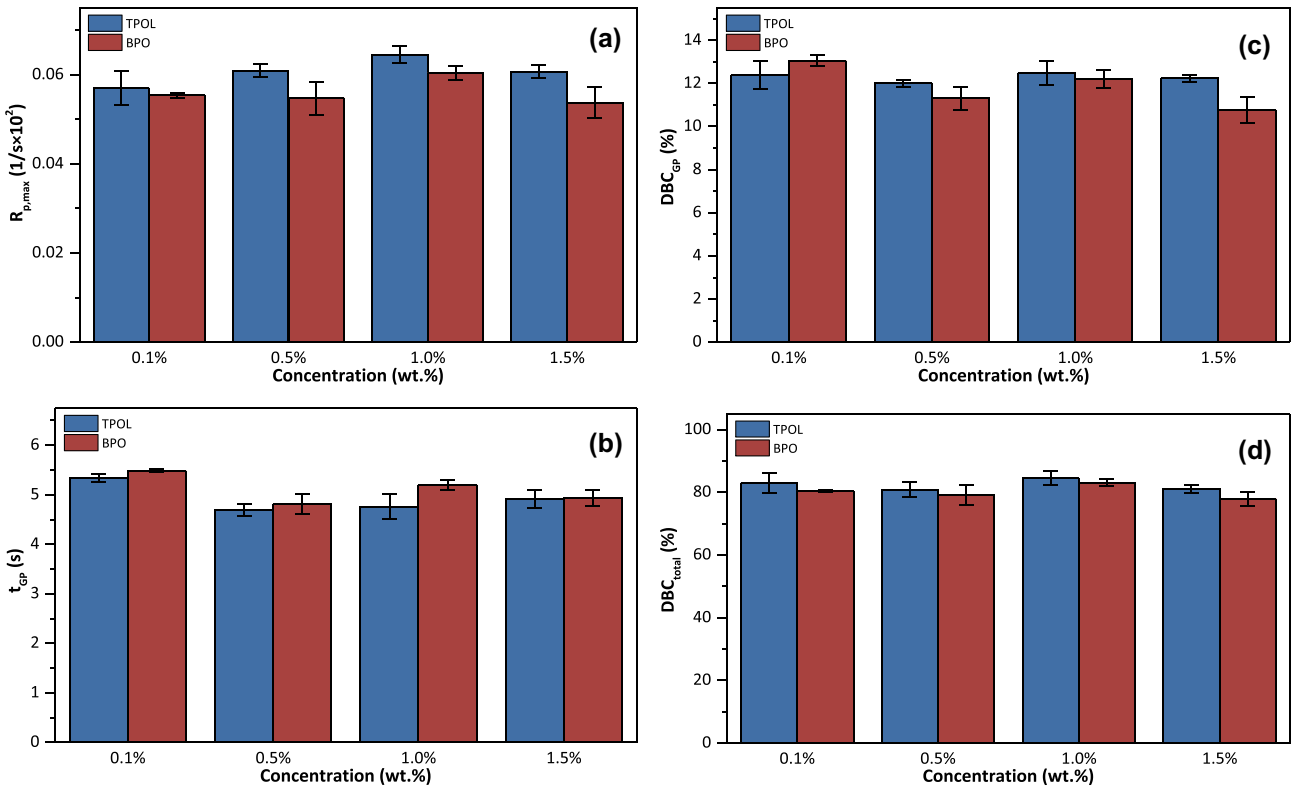

Fig. 2 Photo-reactivity of formulations based on UrDMA/UrA (40/60, wt./wt.) containing different concentrations of TPOL or BPO (0.1–1.5 wt.%) at 25 °C under N_2 atmosphere obtained from photo-DSC data. The intensity of the UV lamp was 0.1 mW/cm^2

are being absorbed, thus C_d is high but *DBC* is low. On contrary, high photo-initiator concentration results in major photon absorption, hence C_d is low but *DBC* is high. Each formulation was dropped on a glass slide (Fig. S1 in SI) and photo-cured on a DLP 3D printer under different UV (365 nm) intensities and exposure times (Fig. 3). For each formulation, employing higher irradiation intensity and longer exposure time increased C_d. When the photo-initiator concentration, irradiation intensity, and exposure time were not adequate to reach the gel point, the formulations did not photo-cured and C_d was zero (BPO 0.1% and TPOL 1.0%). The formulation with 1 wt.% of TPOL presented higher C_d compared to the formulation with 1 wt.% of BPO, especially at higher irradiation intensities and longer exposure times, which can be attributed to the lower molar extinction coefficient of TPOL (145 L/mol·cm at 365 nm) compared to that of BPO (500 L/mol·cm at 365 nm). As expected, the formulations based on BPO with a large molar extinction coefficient (500 L/mol·cm at 365 nm) allow a more controllable photo-curing process. C_d was improved by increasing the BPO concentration from 0.1 to 0.5 wt.% and then decreased at 1.0 and 1.5 wt.%. BPO molecules can absorb the UV light and limit the light penetration depth into the formulations, thus the photo-curing only occurs near the surface of the formulations (BPO 1.0% and BPO 1.5%) [18].

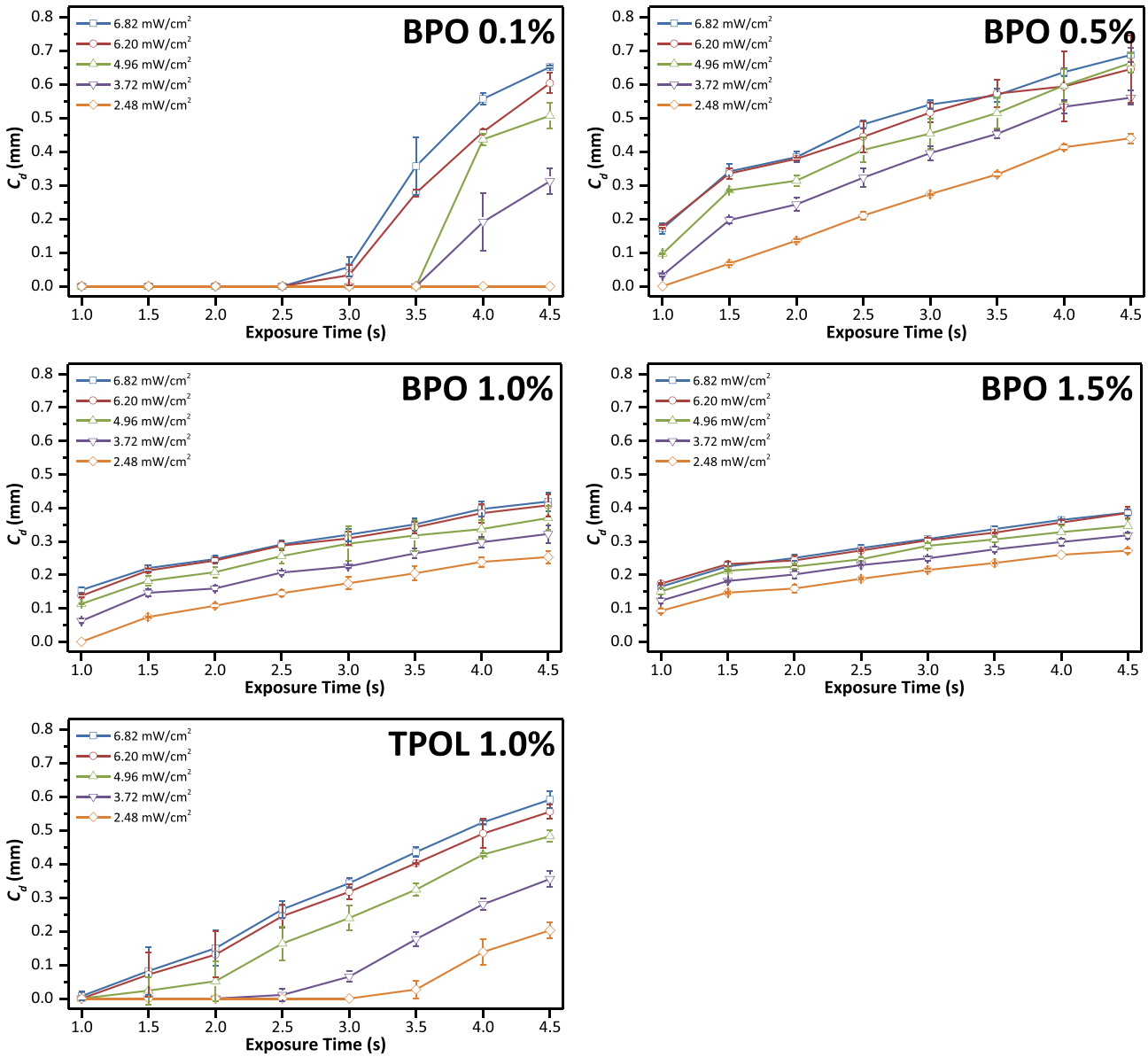

Fig. 3 Photo-curing depth under different UV (365 nm) intensities and exposure times for formulations based on UrDMA/UrA (40/60, wt./wt.) containing different concentrations of TPOL or BPO (0.1–1.5 wt.%) at 25 °C

The formulation with 1 wt.% of BPO was selected as the optimum formulation for 3D printing the objects. For 3D printing with a layer thickness of $\Delta z = 100$ µm, the optimal UV (365 nm) intensity and exposure time were determined as 3.72 mW/cm^2 and 3.0 s, respectively. The shrinkage of the formulation in the course of the 3D printing process was determined as 0.81% for the *X*-direction and 0.91% for the *Y*-direction. Several complex CAD models were designed and successfully 3D printed (Fig. 4). The 3D printed objects were flexible and in good shape.

Post-curing

Post-curing the 3D printed objects can raise the *DBC* and improve their mechanical strength, dimensional stability, and biocompatibility. Both thermal and UV treatments have been used commonly as the post-curing processes. UV treatment is through polymerizing the uncured double bounds under a broad-band UV irradiation. The 3D printed objects were washed twice with fresh isopropanol and post-cured under a high-intensity UV lamp for different exposure times. In the course of post-curing for 5 min, the 3D printed objects got stiffer and their light yellow color disappeared due to the complete decomposition of photo-initiator molecules, while several cracks appeared on their surface (Fig. 5a). During the post-curing process, the double bonds further polymerized resulting in additional shrinkage and consequently mechanical internal stress within the 3D printed objects, which could not be released immediately and caused fractures, especially on their surfaces [19–21]. At the same time, the temperature of the 3D printed objects raised sharply under the high-intensity UV lamp, which led to the rapid evaporation of the absorbed isopropanol during the washing step. To avoid surface cracks, the total exposure time of 5 min was split into 5 × 1 min, while the UV lamp was turned off for 2 min between each irradiation sequence. This routing led to the continuous stiffening of the 3D printed objects and the gradual disappearance of their light yellow color, while no surface cracks were observed (Fig. 5a).

The progress of photo-polymerization in the course of 3D printing and post-curing steps was studied through FTIR spectroscopy (Fig. 5b). The formulation of UrDMA/UrA (40/60, wt./wt.) with BPO (1.0 wt.%) displayed the characteristic peaks for urethane-acrylates 3343 cm^{-1} (N−H, ν) [10, 22], 2958 and 2872 cm^{-1} (C−H, ν), 1702 cm^{-1} (C = O,

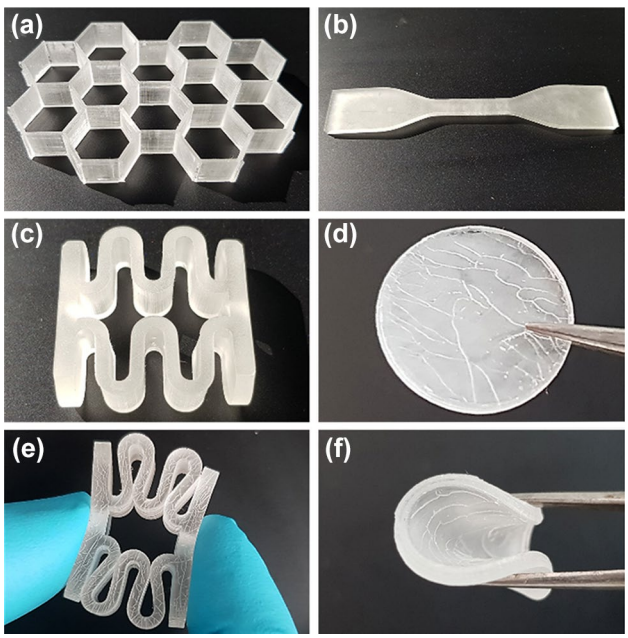

Fig. 4 Images of 3D printed flexible objects; hexagonal **a**, bone-shape specimen **b**, spring **d** and **e**, and disk (Ø: 15 mm, **d** and **f**)

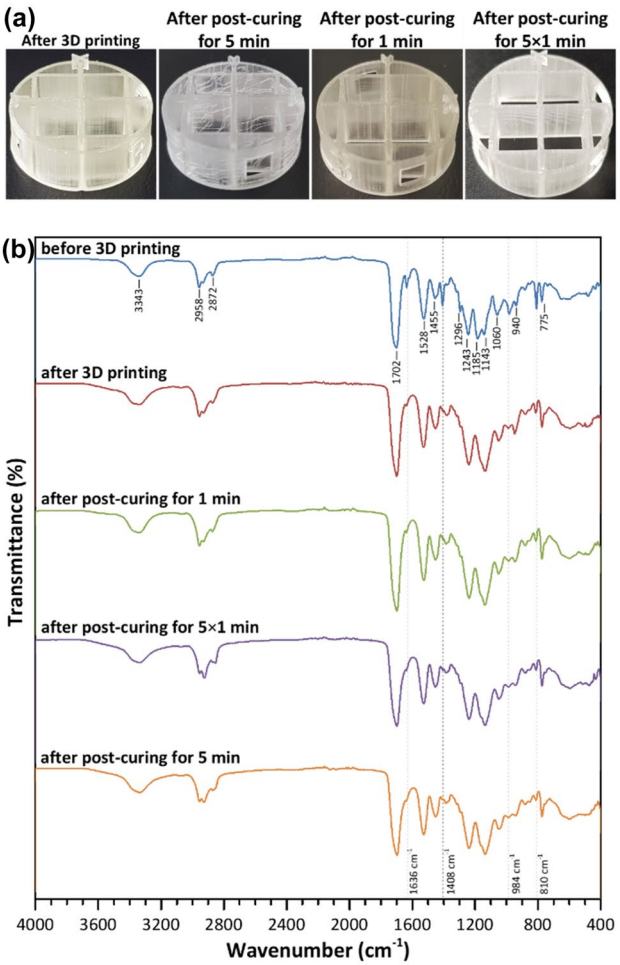

Fig. 5 **a** Images of a 3D printed object based on a formulation of UrDMA/UrA (40/60, wt./wt.) with BPO (1.0 wt.%) before and after post-curing for different times. **b** FTIR spectra of formulation and 3D printed specimen before and after 3D printing or post-curing for different times

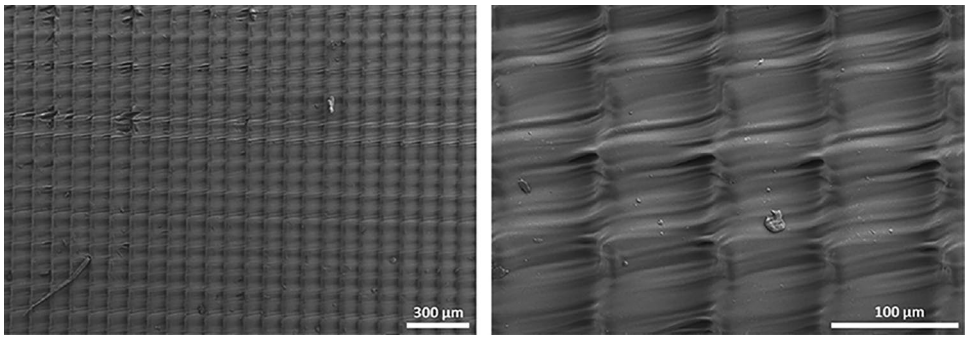

Fig. 6 SEM images for the cross-section of a 3D printed sample

ν) [10, 23–25], 1636 cm^{-1} (C = C, ν) [10], 1528 cm^{-1} (CON−H, δ and CO−NH, ν) [10, 22], 1455 cm^{-1} (CH_3, δ) [10], 1408 (= CH_2, δ, scissoring), 1296 cm^{-1} (CH_2, δ) [10], 1243 cm^{-1} (C−N, ν), 1185, and 1143, and 1060 cm^{-1} (C−O, δ) [10], and 984 and 810 cm^{-1} (= CH, δ, out-of-plane). The intensity of peaks for double bonds at 1636, 1408, 984, and 810 cm^{-1} was gradually decreased as the formulation was photo-cured during the 3D printing process and later during the post-curing process for a longer time. The peaks almost disappeared similarly when the 3D printed objects were post-cured for 5 × 1 or 5 min, meaning equal *DBC*. Thus, splitting the post-curing time is a good solution to improve the *DBC* and consequently the stiffness of the 3D printed objects without destroying their quality.

Surface morphology

SEM images for the cross-section of the 3D printed objects exposed striped features indicating the individual layers formed during the continuous layer-by-layer 3D printing process (Fig. 6). The distance between the strips was approximately 100 µm, equal to the predetermined Δz value for each layer. Moreover, the interface between the layers was observed as intensive and contrasting vertical stripes.

Mechanical properties

Changing the ratio of multi-functional crosslinker to mono-functional reactive diluents in photo-inks and altering the

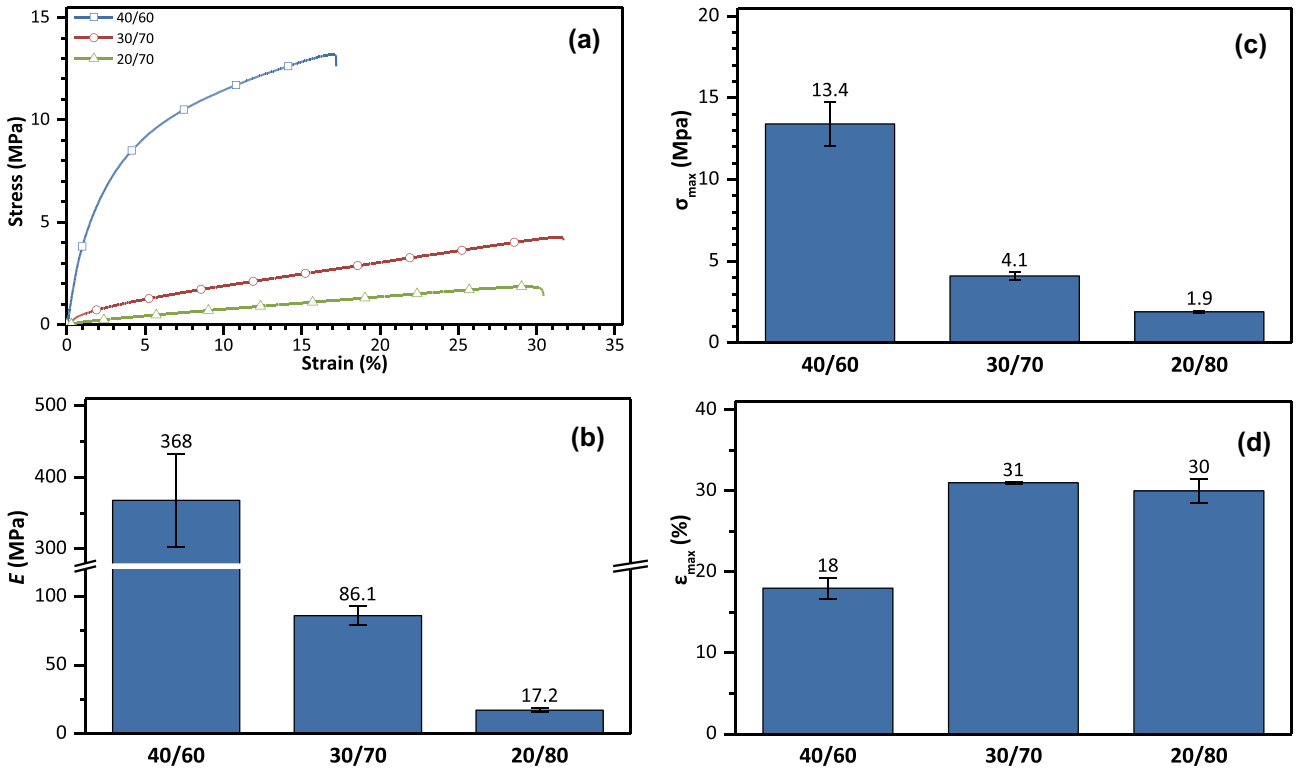

Fig. 7 Stress–strain curves, maximum tensile (σ_{max}, **a**), maximum elongation (ε_{max}, **b**), and tensile modulus (E) of the 3D printed bone-shaped specimens based on UrDMA/UrA mixtures containing TPOL (1 wt.%)

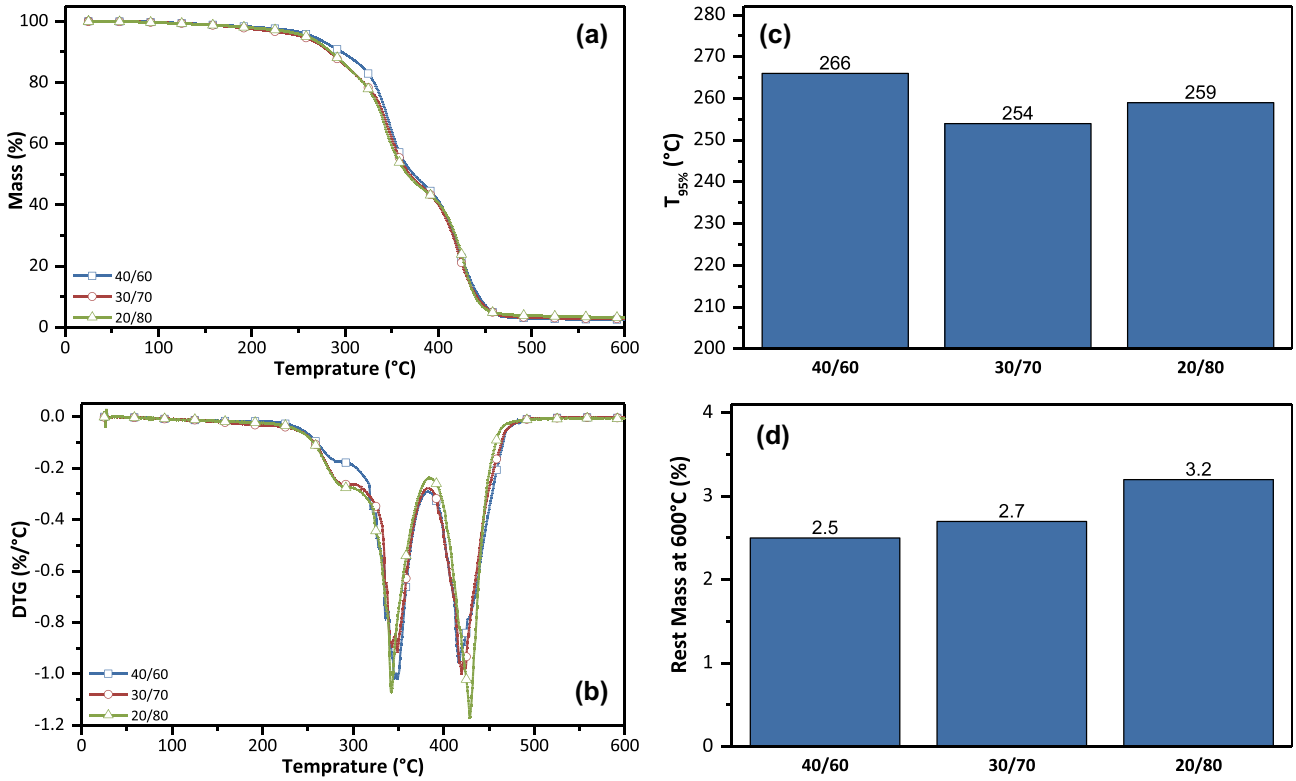

Fig. 8 Thermal stability of the 3D printed samples based on UrDMA/UrA mixtures containing TPOL (1 wt.%) under N_2 atmosphere at a heating rate of 10 °C/min

average double bound functionality, can affect the mechanical properties of the 3D printed objects [9]. Here, the ratio of UrDMA/UrA in the formulations was changed from 40/60 to 30/70 and 20/80, and the mechanical properties of the corresponding 3D printed bone-shaped samples were studied by determining tensile modulus (E), maximum tensile (σ_{max}), and maximum elongation (ε_{max}), at ambient temperature derived from stress–strain curves (Fig. 7). All samples exposed the typical stress–strain curves of the thermoset polymer, a linear elastic region followed by a failure point without any yield point (Fig. 7a) [26–28]. As expected, increasing the UrA content from 60 to 80% resulted in a decrease in E and σ_{max} values (Fig. 7b–c) and an increase in ε_{max} values (Fig. 7d) [9]. Reducing the average double bound functionality in photo-inks leads to a fall in crosslinking density for the corresponding polymeric network. Similar observations were previously reported about photo-cured mono- and di-functional urethane-acrylates [9, 29].

Thermal stability

The thermal stability of the 3D printed objects based on UrDMA/UrA mixtures (40/60, 30/70, and 20/80) was evaluated by TGA (Fig. 8). All samples underwent a two-step thermal degradation profile with peak temperatures of 340–350 and 410–430 °C (Fig. 8a–b). The first weight loss was due to the thermal degradation of urethane bonds generating primary amine and olefin or secondary amine and carbon dioxide [26, 30]. The second weight loss was related to the thermal degradation of the aliphatic hydrocarbon moieties [26, 30–32]. The onset of thermal degradation ($T_{95\%}$, the temperature at which 5% weight loss took place) was higher for the 3D printed objects based on the UrDMA/UrA mixture of 40/60 (266 °C) due to their higher crosslinking density (Fig. 8c). The char yield (rest mass at 600 °C) was higher for the 3D printed objects based on the UrDMA/UrA mixture of 20/80 (Fig. 8d). This phenomenon was due to the formation of nitrogenous char generated through the decomposition of urethane moieties. The content of urethane moieties for the UrDMA/UrA mixture (40/60, 30/70, and 20/80) was 4.49, 4.53, and 4.57 mmol/g, respectively. Thus, the 3D printed objects based on the UrDMA/UrA mixture of 20/80 with higher urethane content displayed higher char yield (3.2% at 600 °C).

Conclusions

Although kinetics investigations based on photo-DSC results did not show any significant difference between the photo-activity of formulations containing BPO or TPOL

at various concentrations, BPO with a high molar extinction coefficient and thus a lower light penetration depth for the formulations resulted in higher controllability on the layer thickness during the 3D printing process. For the desired layer thickness of 100 µm, employing BPO with a concentration of 1.0 wt.% was optimal. The appearance of surface cracks during the post-curing process could be dissolved by splitting the exposure time (5 min) into short (5×1 min) intervals. By changing the ratio of UrDMA/UrA, a range of mechanical properties, *e.g.* stiffness, flexibility, and hardness, is achievable. Increasing the UrA content decreased E and σ_{max} for the 3D printed objects, where the UrDMA/UrA mixture of 30/70 exhibited the highest ε_{max} value.

Supplementary Information The online version contains supplementary material available at https://doi.org/10.1007/s10965-023-03519-7.

Acknowledgements The authors acknowledge the financial support by the Federal Ministry of Education and Research of Germany in the framework of "ProMatLeben – Polymere" (project number 13XP5087E, PolyKARD).

Funding Open Access funding enabled and organized by Projekt DEAL.

Data availability The raw/processed data used to support the findings of this study are available from the corresponding author upon request.

Declarations

Conflicts of interest There are no conflicts to declare.

References

1. Chua CK, Leong KF (2017) 3D printing and additive manufacturing: principles and applications, The 5th edition of Rapid prototyping : principles and applications. World Scientific Publishing Co. Pte. Ltd, Singapore; New Jersey
2. Radmanesh S, Shabangiz S, Koupaei N, Hassanzadeh-Tabrizi SA (2022) 3D printed bio polymeric materials as a new perspective for wound dressing and skin tissue engineering applications: a review. J Polym Res 29:50. https://doi.org/10.1007/s10965-022-02899-6
3. Layani M, Wang X, Magdassi S (2018) Novel materials for 3D printing by photopolymerization. Adv Mater 30:1706344. https://doi.org/10.1002/adma.201706344
4. Talianov PM, Rzhevskii SS, Pankin DV et al (2021) Structural features of functional polysiloxanes radical and ionic photo-curing for laser printing applications. J Polym Res 28:37. https://doi.org/10.1007/s10965-021-02409-0
5. Gojzewski H, Guo Z, Grzelachowska W et al (2020) Layer-by-layer printing of photopolymers in 3D: How weak is the interface? ACS Appl Mater Interfaces 12:8908–8914. https://doi.org/10.1021/acsami.9b22272
6. Pooput K, Channasanon S, Tesavibul P et al (2020) Photocurable elastomers with tunable mechanical properties for 3D digital light processing printing. J Polym Res 27:322. https://doi.org/10.1007/s10965-020-02289-w
7. Jockusch S, Turro NJ (1998) Phosphinoyl radicals: Structure and reactivity. A laser flash photolysis and time-resolved ESR investigation. J Am Chem Soc 120:11773–11777. https://doi.org/10.1021/ja982463z
8. Jockusch S, Koptyug IV, McGarry PF et al (1997) A steady-state and picosecond pump-probe investigation of the photophysics of an acyl and a bis(acyl)phosphine oxide. J Am Chem Soc 119:11495–11501. https://doi.org/10.1021/ja971630c
9. Bakhshi H, Kuang G, Wieland F, Meyer W (2022) Photo-curing kinetics of 3D-printing photo-inks based on urethane-acrylates. Polymers 14:2974. https://doi.org/10.3390/polym14152974
10. Singh N, Bakhshi H, Meyer W (2020) Developing non-isocyanate urethane-methacrylate photo-monomers for 3D printing application. RSC Adv 10:44103–44110. https://doi.org/10.1039/D0RA06388F
11. Eibel A, Fast DE, Gescheidt G (2018) Choosing the ideal photoinitiator for free radical photopolymerizations: predictions based on simulations using established data. Polym Chem 9:5107–5115. https://doi.org/10.1039/C8PY01195H
12. Dietlin C, Trinh TT, Schweizer S et al (2019) Rational design of acyldiphenylphosphine oxides as photoinitiators of radical polymerization. Macromolecules 52:7886–7893. https://doi.org/10.1021/acs.macromol.9b01724
13. Dietliker K (2002) A compilation of photoinitiators commercially available for UV today. Sita Technology Ltd, London, UK
14. Mayerhöfer TG, Pahlow S, Popp J (2020) The bouguer-beer-lambert law: Shining light on the obscure. ChemPhysChem 21:2029–2046. https://doi.org/10.1002/cphc.202000464
15. Melchels FPW, Feijen J, Grijpma DW (2010) A review on stereolithography and its applications in biomedical engineering. Biomaterials 31:6121–6130. https://doi.org/10.1016/j.biomaterials.2010.04.050
16. Xu Y, Wang H, Xie D (2018) Preparation of new low viscosity urethane dimethacrylates for dental composites. J Biomater Sci Polym Ed 29:1011–1025. https://doi.org/10.1080/09205063.2017.1364098
17. Soreni-Harari M, St. Pierre R, McCue C et al (2020) Multimaterial 3D printing for microrobotic mechanisms. Soft Rob 7:59–67. https://doi.org/10.1089/soro.2018.0147
18. Lee JH, Prud'homme RK, Aksay IA (2001) Cure depth in photopolymerization: Experiments and theory. J Mater Res 16:3536–3544. https://doi.org/10.1557/JMR.2001.0485
19. Schoerpf S, Catel Y, Moszner N et al (2019) Enhanced reduction of polymerization-induced shrinkage stress via combination of radical ring opening and addition fragmentation chain transfer. Polym Chem 10:1357–1366. https://doi.org/10.1039/C8PY01540F
20. Karalekas D, Aggelopoulos A (2003) Study of shrinkage strains in a stereolithography cured acrylic photopolymer resin. J Mater Process Technol 136:146–150. https://doi.org/10.1016/S0924-0136(03)00028-1
21. Karalekas D, Rapti D, Gdoutos EE, Aggelopoulos A (2002) Investigation of shrinkage-induced stresses in stereolithography photocurable resins. Exp Mech 42:439–444. https://doi.org/10.1007/BF02412150

22. Bakhshi H, Agarwal S (2016) Dendrons as active clicking tool for generating non-leaching antibacterial materials. Polym Chem 7:5322–5330. https://doi.org/10.1039/C6PY01105E
23. Visser D, Bakhshi H, Rogg K et al (2022) Green chemistry for biomimetic materials: Synthesis and electrospinning of high-molecular-weight polycarbonate-based nonisocyanate polyurethanes. ACS Omega 7:39772–39781. https://doi.org/10.1021/acsomega.2c03731
24. Yari A, Yeganeh H, Bakhshi H, Gharibi R (2014) Preparation and characterization of novel antibacterial castor oil-based polyurethane membranes for wound dressing application: Preparation and characterization of novel antibacterial co-based polyurethane membranes. J Biomed Mater Res 102:84–96. https://doi.org/10.1002/jbm.a.34672
25. Yari A, Yeganeh H, Bakhshi H (2012) Synthesis and evaluation of novel absorptive and antibacterial polyurethane membranes as wound dressing. J Mater Sci Mater Med 23:2187–2202. https://doi.org/10.1007/s10856-012-4683-6
26. Bakhshi H, Yeganeh H, Yari A, Nezhad SK (2014) Castor oil-based polyurethane coatings containing benzyl triethanol ammonium chloride: synthesis, characterization, and biological properties. J Mater Sci 49:5365–5377. https://doi.org/10.1007/s10853-014-8244-x
27. Bakhshi H, Yeganeh H, Mehdipour-Ataei S (2013) Synthesis and evaluation of antibacterial polyurethane coatings made from soybean oil functionalized with dimethylphenylammonium iodide and hydroxyl groups. J Biomed Mater Res 101A:1599–1611. https://doi.org/10.1002/jbm.a.34461
28. Bakhshi H, Yeganeh H, Mehdipour-Ataei S et al (2013) Synthesis and characterization of antibacterial polyurethane coatings from quaternary ammonium salts functionalized soybean oil based polyols. Mater Sci Eng C 33:153–164. https://doi.org/10.1016/j.msec.2012.08.023
29. Deng Y, Li J, He Z et al (2020) Urethane acrylate-based photosensitive resin for three-dimensional printing of stereolithographic elastomer. J Appl Polym Sci 137:49294. https://doi.org/10.1002/app.49294
30. Bakhshi H, Yeganeh H, Mehdipour-Ataei S et al (2013) Polyurethane coatings derived from 1,2,3-triazole-functionalized soybean oil-based polyols: Studying their physical, mechanical, thermal, and biological properties. Macromolecules 46:7777–7788. https://doi.org/10.1021/ma401554c
31. Bakhshi H, Agarwal S (2017) Hyperbranched polyesters as biodegradable and antibacterial additives. J Mater Chem B 5:6827–6834. https://doi.org/10.1039/C7TB01301A
32. Ahmadabad FK, Pourayoubi M, Bakhshi H (2017) Novel Keggin-type polyoxometalate nanocatalysts for Michael addition polymerizations. Mater Chem Phys 199:79–87. https://doi.org/10.1016/j.matchemphys.2017.06.045